Nanotechnology-Enhanced Filtration:

SCHN 135 Sol-Gel Treatment Reduces Aerosol Particle Penetration Through HVAC Filters and Face Masks

B. Varon[1,4], B. N. Yagmur[2,4], A. Lostaunau[3,4], D. Mayahi[4], A. J. Taylor[4], S.A. Curran[4,5]

[1]Department of Psychological, Health, & Learning Sciences, College of Education, McElhinney Hall 3623 Cullen Blvd., 3001, University of Houston, Houston 77204-5023, Texas

[2]Department of Biology and Biochemistry, College of Natural Sciences and Mathematics, Science and Research Building 2, 3455 Cullen Blvd #342, University of Houston, Houston 77204, Texas

[3]Department of Psychology, College of Liberal Arts and Social Sciences, 3553 Cullen Blvd, University of Houston, Houston 77204, Texas

[4]Curran's Nanophysics Research Group, University of Houston, Science & Research Building 1, 3507 Cullen Blvd., Houston, TX 77204 USA

[5]Physics Department, Science and Research Building 1, University of Houston, Houston, 77204, Texas

Abstract

Airborne respiratory particles represent a vital pathway in the transmission of respiratory diseases, especially in indoor environments where suspended particles may be transported and recirculated through mechanical ventilation systems. The key to reducing the risk of aerosol virus-containing particles is stopping the cycle of cross-contamination at the start, preventing the cycle from ever occurring. By halting the cycle of cross-contamination of aerosol particles at the beginning, this method decreases an individual's chance of being infected and potentially proposing an alternative solution. Filtration barriers, including Heating, Ventilation, and Air Conditioning (HVAC) filters and face masks, can reduce exposure to aerosol particles; however, their performance varies depending on the size of the particle, airflow conditions, and the filtration material. This study investigates whether surface modification using SCHN 135, a hydrophobic sol-gel nanocoating, could reduce the downstream transport and deposition of aerosol particles through commonly used

filters and face masks. Across all three filtration materials tested, SCHN 135 treated samples proved to have lower downstream deposition than their corresponding untreated conditions, with a relative decrease ranging from 71.6% to 98.2% by visible analysis and 56.8% to 89.6% by microscopic analysis.

Introduction

Every breath, cough, and sneeze release respiratory particles into the air. When an individual is sick with a respiratory virus, their respiratory particles carry infectious material that creates a pathway for transmission to others [1,2]. Respiratory emissions do not simply exist as a single class, like “droplets” or “aerosols”, they span a very broad and multimodal range of particle sizes that are created by an individual’s respiratory tract [2, 3]. This distinction is important because the virus itself is not transmitted through the air as an isolated virion; rather, the viral material is encapsulated within respiratory fluid particles. The airborne behavior of each particle is determined by the size and composition of the “carrier” particle. Studies on influenza patients have shown that viral material is present in aerosol particles throughout the respirable range, including particles smaller than 1 µm, and viable influenza A has also been found in aerosols produced by coughing [4,5]. Once released into the surrounding air, larger particles >100 µm tend to fall to the ground in under 5 seconds and travel no farther than 1 meter. Whereas smaller particles like <100 µm travel farther and <5 µm can stay suspended in the air for hours and travel well beyond 1 meter, making them optimally sized for cross-contamination for others to inhale [2,3]. This is particularly significant in indoor settings, where people can potentially be exposed to the same air for extended periods.

Mechanical ventilation continuously transports, mixes, and in some systems, recirculates the airborne particles. As a result, there are multiple levels of protection against respiratory aerosol

exposure. While masks and respirators offer an individual-level filtration barrier at the interface between a person and their surroundings, HVAC filters offer a building-level barrier designed to remove suspended particles from circulating air [6,7,8]. When combined, these devices offer two significant opportunities to stop respiratory aerosols from spreading through occupied spaces before they are ever redistributed back into the air.

However, total particle removal is not guaranteed by the presence of a filtration barrier. The size, aerodynamic behavior, structure, and characteristics of the filter, as well as the speed at which air passes through it, all influence whether a particle is collected [6,9,10]. HVAC filters are commonly graded by the Minimum Efficiency Reporting Value (MERV), which classifies the filter's performance in removing certain particulates from the air. MERV ratings range from 1 to 16, with increasing ratings indicating greater particle removal efficiency. MERV 8 filters represent the lower end of filtration efficiency for residential uses, making their performance relevant to everyday indoor environments. For example, MERV 8 filters are primarily utilized for their performance against larger particles in the 3–10 µm range, consequently they are substantially more vulnerable to particles in the smaller 0.3–1 µm and 1–3 µm ranges, the typical sizes of airborne respiratory particles [6,9].

Research into HVAC filtration and viral transmission found that filtration can reduce airborne viral cross-contamination, but that performance directly varies on the filter efficiency and operating conditions [6]. At the individual level, the same problem exists. Experimental testing of commercial mask materials has shown that there is a considerable amount of size-dependent filtration, with N95 respirators outperforming the lower grade masks, but with still a measurable penetration. The performance of masks and respirators, similar to the efficiency of filters, is dependent on aerosol size, airflow, material, and testing conditions [7,10]. Thus, whether the goal is to protect shared indoor environments through HVAC filtration or offer filtration at the

individual level through masks, the problem remains the same: the protective barriers put in place to prevent the passage of aerosol particles are still allowing penetration. Increasing the filter density or getting a higher-level MERV filter to improve particle removal efficiency can work; however, this does introduce some practical considerations. Not only will the increased airflow resistance require higher-power HVAC systems, but it will also increase energy demands, making this method challenging for the general population. This raises the question: rather than replacing existing filters and filtration materials, can the surface of the material itself be modified to enhance its ability to remove aerosol particles? By answering this question, material engineering can be used to improve both individual and building-level filtering systems, laying the groundwork for further research into surface treatments based on nanotechnology as an alternative aerosol capture mechanism [11].

Mechanisms of Particle Capture

The transport and behavior of airborne particulates vary depending on their size and location. Brownian motion, named after Robert Brown, describes the irregular movement of particles based on collisions with surrounding molecules [12,13]. In filtration, this random motion becomes important for smaller aerosol particles because it causes them to move outside of their airflow streamlines, increasing the chance to make contact with a filter fiber [12,14]. Therefore, Brownian diffusion represents another capture mechanism for smaller aerosol particles [14]. Particulates are capable of interacting with filtration systems in two ways. Inertial impaction is the mechanism where particles with enough momentum and inertia divert from the air streamlines, resulting in them impacting the fiber [14,15,16]. Typically, these particles are larger in size and therefore, have more momentum compared to smaller particles and are easier to catch within the fibers of filters.

Interception is the mechanism for smaller particles, where they maintain the air streamline

but become close enough to the fibers and are susceptible to forces and stick. These forces on filters are microscopic Van der Waals forces and overcome the kinetic energy within the particle, causing it to be captured by the fibers within the filter [17]. The most penetrating particle size (MPPS) refers to the particle size at which the fiber filters have their lowest collection efficiency and therefore the greatest particle penetration [18]. Reducing fiber diameter allows more fibers and a greater total fiber surface area within the filter, creating more opportunities for particles to interact with and be captured by the fibers [14,18]. However, higher rated filters are more cost-heavy compared to lower rated filters. To combat this issue, attention was diverted towards a surface-mechanical solution to enhance filtration efficiency utilizing a lower rated filter to prevent the passage of particulates and showcase the capabilities of SCHN 135.

Properties of SCHN 135

SCHN 135, synthesized from Integricote™, is a sol-gel based nanocoating that acts as a hydrophobic surface and repels polar liquids [19, 20, 21]. Initially designed for carpets and fabrics, SCHN 135 was tested to determine its effectiveness on filtration systems and variations of masks. Sol-gel is termed for the process of microparticles in a liquid joining together, under controlled conditions, and linking with one another to form a network [20, 22, 23]. Its hydrophobic nature is a result of cross-linking, where covalent bonds are formed to ultimately create a three-dimensional network, enhancing stability of the polymer [19]. This cross-linking behavior also prevents degradation of the material and allows for SCHN 135 coatings to be viable without interfering with the mechanisms of the material it coats.

Study Rationale and Objectives

The COVID-19 pandemic demonstrated the consequences that can result from the rapid spread of respiratory pathogens through shared environments, causing millions of deaths worldwide and

placing unprecedented strain on our healthcare systems [24,25,26,27]. As one of the major U.S. cities hit hardest by COVID-19, New York City recorded over 11,000 deaths by April 15, 2020, accounting for roughly 43% of all U.S. fatalities at that time [26]. Due to the rapid spread of the virus, the entire world shut down and halted all operations. Hospitals overcrowded with patients infected with the virus, resulting in a shortage of personal protective equipment (PPE), rendering healthcare workers susceptible to contracting the virus. As the pandemic progressed, shortages continued in hospitals with limited ICU beds and ventilators being available for patients [26]. The scale of the pandemic raised an important preventative question: could the magnitude of this devastating outbreak have been reduced? This question is particularly relevant to HVAC systems and PPE, which represent two opportunities to intercept respiratory particles during transmission.

Related preliminary work by Wang et al. investigated a different hydrophobic nanocoating, designated MVTR-A1/Capture Coating, using thermally inactivated SARS-CoV-2 in a controlled airflow filtration system [28]. In the study, experimental HVAC filters were positioned upstream of separate collector filters, and viral material was recovered downstream and quantified using RT-qPCR. The results suggested reduced downstream viral material for the treated condition. Evaluating such surface modifications can be done by using a fluorescent tracer to examine particle transport and containment while allowing deposition to be visualized and quantified. Johnson and Lynch demonstrated that micrometer scale fluorescent microspheres could serve as surrogates for pathogenic bioaerosols, be recovered on collection filters, and quantified to assess airborne containment [29]. Fluorescent Glo Germ materials have been used experimentally to visualize the transport of respiratory particles. Patel et al. characterized Glo Germ MIST as one of several fluorescent simulators used to investigate respiratory droplet dispersion [30]. In these studies, an aerosol challenge is used to evaluate the effects of a simulated respiratory aerosol on the target substrate. Shah et al. applied this method using Glo Germ MIST to track particle movement,

showing that introducing physical barriers like masks significantly altered downstream dispersion [31]. These studies support the use of liquid tracers in aerosol experiments while also highlighting an important limitation: Glo Germ MIST does not completely represent the particle structure or biological properties of a naturally occurring respiratory virus [30,31]. However, Glo Germ MIST is advertised to produce particles within the 3–5 μm range, which overlaps with the size range of respiratory aerosols capable of carrying viral material; therefore, it provides a useful physical tracer for aerosol transport but should not be considered a direct substitute for an infectious virus [32].

Accordingly, the present study investigates whether the modification of filtration media with SCHN 135, alters the downstream transport of fluorescent particulate challenge under controlled airflow. This study uses Glo Germ MIST as a nonbiological fluorescent tracer to quantify material recovered downstream of untreated and SCHN 135-treated filtration media. Three categories of filtration were examined: 1-inch MERV 8 HVAC filters, disposable painter's masks, and N95 respirators. Treated and untreated conditions are challenged under matched and controlled experimental parameters within each experimental group, and transmitted fluorescent particles are recovered on downstream collector filters. Depositions are evaluated and quantified on two scales using UV-visible imaging and microscopic images. The central hypothesis of this study is that sol-gel-treated filtration media will produce lower downstream fluorescent deposition than their corresponding untreated conditions. The study is therefore designed as a particle retention comparison rather than a measurement of filtration efficiency or antiviral activity. If treatment consistently reduces downstream deposition across multiple filtration substrates, the findings could provide a physical basis for subsequent studies using standardized aerosol challenges and appropriately controlled biological aerosols to determine whether the observed effect extends to virus-containing airborne particles.

Materials and Methods



Figure 1. *Experimental HVAC apparatus used for the study. Airflow proceeded from right to left through the experimental filter (treated or untreated), followed by the downstream collector filter used for deposition analysis, a secondary cleanup filter for residual material capture, and the AC Infinity inline fan.*

Materials and Filter Treatment

Three classes of filtration media were evaluated under untreated and sol-gel treated conditions: 1-inch TrueBlue and Filterbuy MERV 8 HVAC filters, disposable HDX Dust/Povlo painter's masks, and 3M Aura N95 respirators. Treated samples were uniformly coated with the experimental hydrophobic sol-gel formulation SCHN 135 using a spray bottle and allowed to dry for 24 hours before testing. Fluorescent particle challenges were conducted using the Glo Germ MIST Kit Basic [32]. The challenge material was used directly as supplied, without dilution, and was dispensed using the MIST Spray Canister included with the kit. Fluorescent deposition was visualized using the supplied 21 LED ultraviolet flashlight included in the Glo Germ kit.

Filtration Set-Up

Airflow was generated using an AC Infinity CLOUDLINE T10 inline duct fan with a 10-inch duct diameter and a manufacturer-rated maximum airflow of 1201 CFM [33]. Based on the duct area,

the maximum estimated air velocity was approximately 11.2 m/s. Controller setting 5 was treated as approximately 50% of the maximum fan speed, giving an estimated air velocity of approximately 5.6 m/s. This value represents an estimation rather than a directly measured air velocity. For each trial, the experimental filter or mask was placed upstream of the clean collector filter so that the fluorescent materials passing through the test material could be recovered downstream. Treated and untreated samples within each filter material were evaluated using the same experimental configuration.

Table 1. *Experimental conditions challenged with the Glo Germ*

Test Material	**Treatment**	**Source Distance (cm)**	**Challenge Duration (s)**	**Fan Setting**
1-inch MERV 8	Untreated	30 cm	10 s	Speed 5
1-inch MERV 8	SCHN 135 Treated	30 cm	10 s	Speed 5
Painter's Mask	Untreated	15 cm	5 s	Speed 5
Painter's Mask	SCHN 135 Treated	15 cm	5 s	Speed 5
3M Aura N95	Untreated	15 cm	5 s	Speed 5
3M Aura N95	SCHN 135 Treated	15 cm	5 s	Speed 5

Fluorescence Imaging and Particle Quantification

After each sample was challenged with Glo Germ, the downstream collector filter was examined under the UV light. Fluorescent deposits visible throughout the whole filter were documented and counted as the visible deposition.

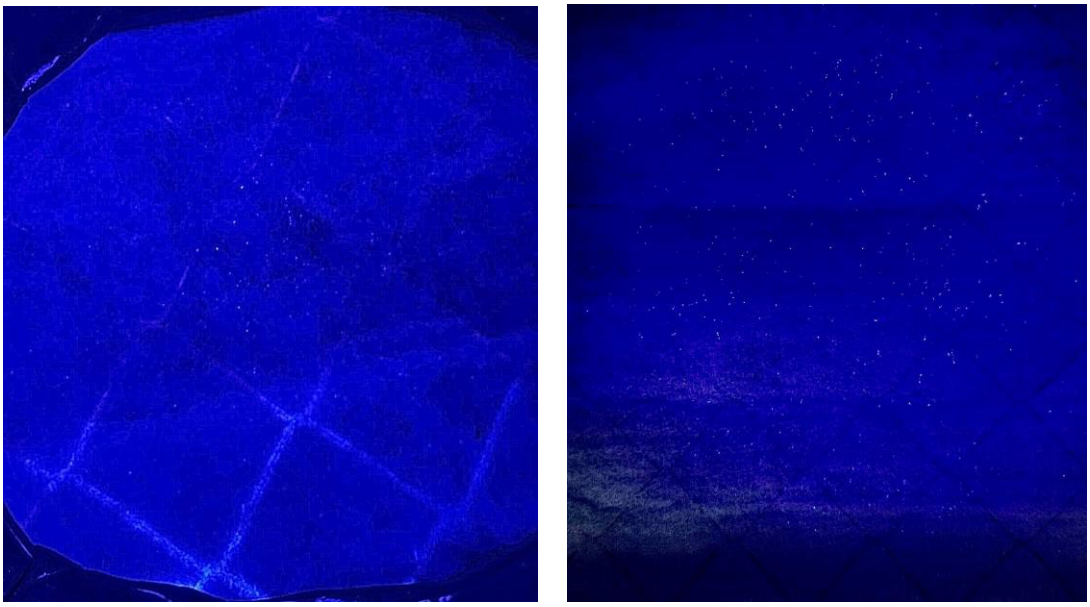


Figure 2. *UV-visible particles in the center of the collector filter¸ mask collector (left) and filter collector (right)*

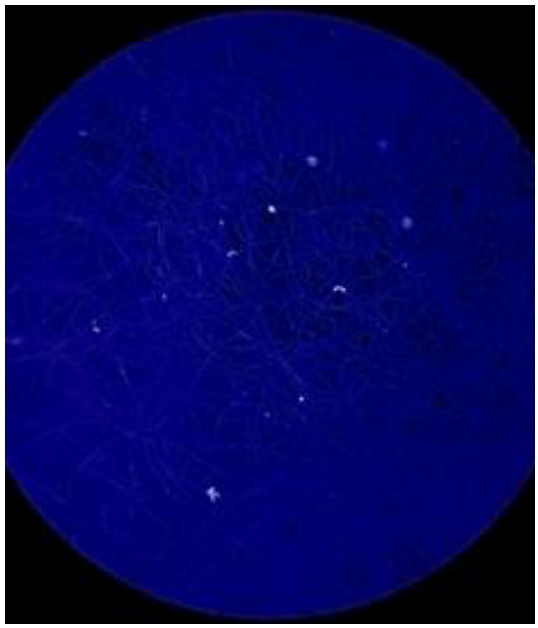


Figure 3. *Microscopic images of collector filters obtained to quantify Glo Germ particles*

Microscopic examination was subsequently used to quantify fluorescent particles that could not be seen macroscopically. Each microscope image, as shown in Figure 4, represented approximately 0.5 x 0.5 cm of the area of the collector filter. Sixteen microscopic fields corresponded to one 2 x 2 cm sampling region, and the collector filter surface contained 36

sampling regions. The downstream collector filter was imaged under ultraviolet illumination and processed to improve visualization of fluorescent Glo Germ deposits, a visible particle that lands on a surface and remains detectable, against the filter background. Adjustments were made to the brightness, contrast, and related parameters of the images to enhance the distinction between fluorescent deposits and the filters prior to quantification. Image processing was restricted to the complete image; individual regions or particles were not selectively enhanced, removed, or altered.

Rather the center of each sample was examined, as this was measured to be the area with the highest concentration. This approach is consistent with established standards for quantitative scientific imaging when used for comparison [34]. Equivalent image processing criteria were applied to all experimental conditions, and images were used for quantitative comparison between untreated and SCHN 135-treated samples. Greater downstream fluorescent deposition was interpreted as greater transmission of challenge material through the test medium under the specified experimental conditions, whereas lower downstream deposition indicated reduced transmission.

A separate deposition experiment was performed to approximate the number of particles generated by the Glo Germ MIST spray. Glo Germ was applied to a paper collection surface for 1 second, and the concentrated deposition region was analyzed using the same spatial counting framework used for the analysis of the collector filter. The concentrated area was found to be approximately 25 by 25 cm. An average count of approximately 1,768 deposits was counted per 2 by 2 cm sample region, generating approximately 276,250 fluorescent deposits within the concentrated area. This estimation followed a Fermi-style approach, named after physicist Enrico Fermi, in which a difficult-to-measure total quantity is approximated by measuring a representative smaller region and scaling that value to the full area.

Results

Downstream Fluorescent Deposition

Experiments with Glo Germ were measured by fluorescent deposition on the downstream collector for each trial. Downstream deposition was evaluated on two scales: fluorescent deposits visible on UV-illuminated collector images, and deposits identified via microscopic examination. These were analyzed separately because they represent different detection scales and were not related to one another. Across all three filtration material classes tested, the sol-gel treated samples showed fewer downstream fluorescent deposits than the corresponding untreated condition by both deposition scales. The complete dataset is summarized in Table 2.

Table 2. *Downstream Glo Germ deposition measured following passage through untreated and SCHN 135 treated filtration materials*

Filtration Material	**Treatment**	**UV-visible count**	**Microscopic Count**	**Relative decrease in UV-visible count**	**Relative decrease in microscopic count**
1-inch MERV 8	Untreated	987	405	—	—
1-inch MERV 8	SCHN 135 Treated	18	42	98.2%	89.6%
Painter's Mask	Untreated	148	65	—	—
Painter's Mask	SCHN 135 Treated	42	12	71.6%	81.5%
3M Aura N95	Untreated	31	44	—	—
3M Aura N95	SCHN 135 Treated	4	19	87.1%	56.8%

$$\text{Relative decrease (\%)} = \left(\frac{N_{untreated} - N_{treated}}{N_{treated}}\right) \times 100\%$$

Equation 1

Relative decreases were calculated by each filtration material pair using Equation 1 where N represents the downstream count obtained.

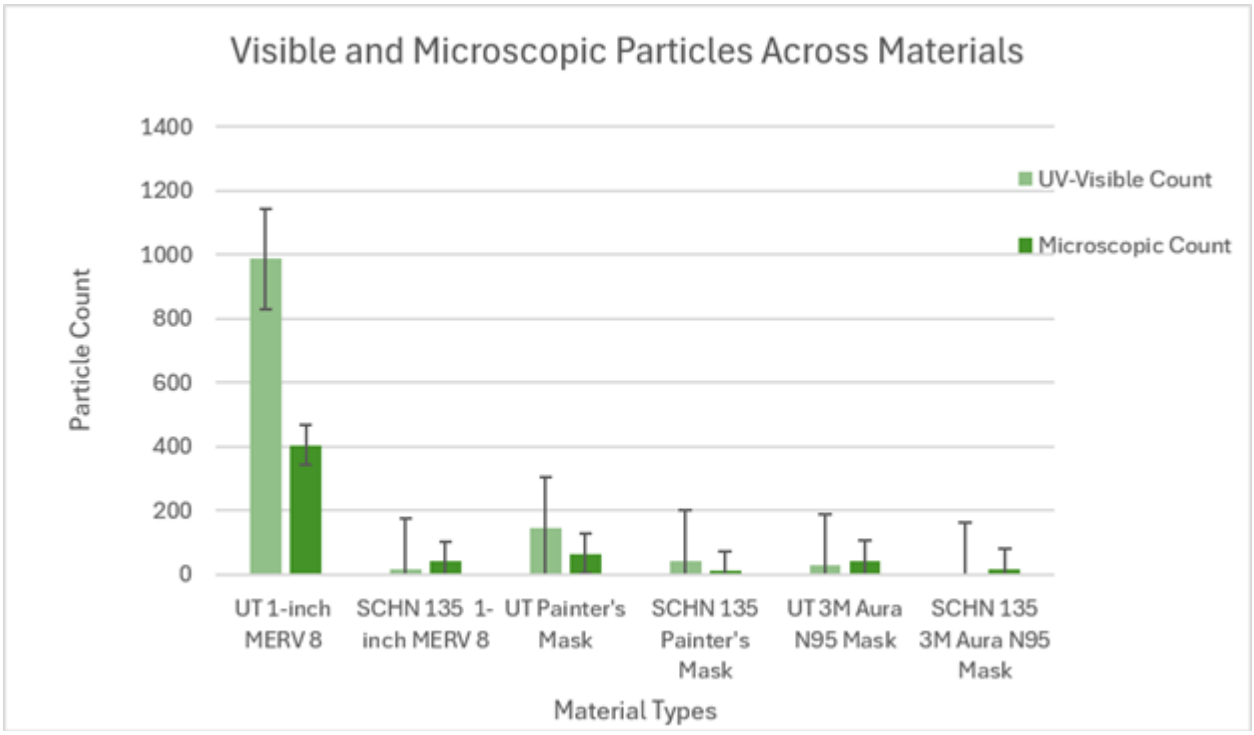


Figure 4. *Representation of visible and microscopic particles across filtration materials tested*

MERV 8 Filter Comparison

The largest difference in downstream fluorescent deposition was observed with 1-inch MERV 8 filters. After the 10-second spray with the Glo Germ at a distance of 30 cm and a fan setting of 5, untreated MERV 8 produced 987 UV-visible deposits on the downstream collector, whereas 18 deposits were recorded for the SCHN 135 treated condition. The treated condition exhibited a 98.2% lower UV-visible downstream count relative to the untreated condition. Microscopic analysis showed the same directional effect. The untreated sample had 405 microscopically detected fluorescent deposits, compared to the 42 in treated samples, corresponding to an 89.6%

relative decrease in microscopic downstream deposition. Thus, both independently evaluated imaging scales showed significantly fewer fluorescent particles on the collector downstream of the treated MERV 8 condition. Even when compared using two different spatial resolutions, the results were in agreement.

Painter's Mask Comparison

A reduction in downstream fluorescent deposition was also observed for the painter's mask experiments. Under matched challenge conditions of 5-second Glo Germ sprays at a distance of 15 cm and a fan setting of 5, the untreated painter's mask showed 148 UV-visible deposits, whereas SCHN 135 treated mask showed 42. This shows a 71.6% decrease in UV-visible downstream deposition for the treated sample. The difference was also clear microscopically, with the untreated mask having 65 particles compared with the 12 for the treated sample. This corresponded to an 81.5% relative decrease in microscopic downstream deposition. The two measurements independently showed the same overall pattern: substantially fewer fluorescent Glo Germ droplets reached the downstream collector when the painter's mask was treated with SCHN 135.

Deposition of Glo Germ Behind Painter's Masks

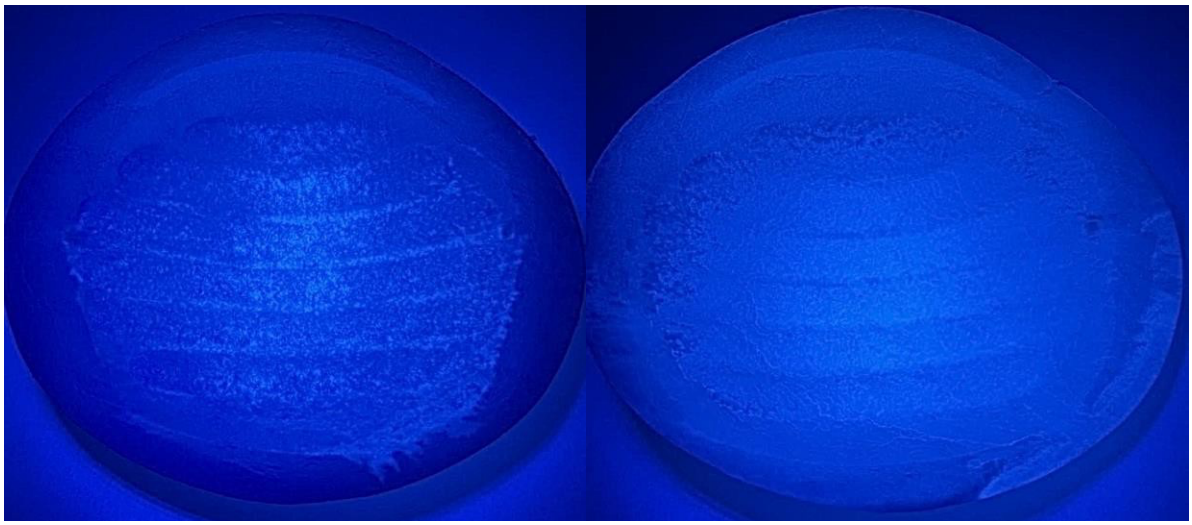


Figure 5. *UV-visible deposition on the back of painter's masks of treated (left) and untreated (right)*

When the back of the painter's masks was seen and imaged using a UV light, the treated mask showed a decrease in the amount of Glo Germ that passed through. This was seen and compared using the amount of the back of the mask that glowed when looked under a UV light. This difference was not clear with the N95 masks, although there were particles that penetrated through; the mask did saturate enough to show full wicking penetration like the painter's mask did.

N95 Mask Comparison

The untreated and treated N95 trials showed a similar difference in downstream fluorescent deposition. After the 5-second Glo Germ challenge at 15 cm and fan setting of 5, there were 31 UV-visible deposits recorded at the downstream filter of the untreated N95 mask, compared with 4 droplets of the SCHN 135-treated N95. This was an 87.1% relative decrease in the UV-visible count. Microscopic examination showed 44 depositions for the untreated N95 mask and 19 droplets for the treated trial, representing 56.8% relative decrease. Although the magnitude of difference was smaller microscopically than in the macroscopic UV analysis, both scales showed a lower downstream fluorescent deposition for the treated sample. The N95 results, therefore, followed the same directional trend observed for the MERV 8 and painter's mask comparisons.

Comparison Across Filtration Materials

A consistent qualitative pattern was seen across the three filtration classes: every SCHN 135-treated condition produced a lower downstream count than its corresponding untreated condition for both the UV-visible and microscopic measurements. The magnitude of the difference between treated and untreated samples varied according to the filtration material and measurement scale. For UV-visible deposition, relative decreases were 98.2% for MERV 8 filters, 71.6% for the painter's mask, and 87.1% for the N95. For microscopic deposition, the corresponding decreases were 89.6%,

81.5%, and 56.8%, respectively.

When looked at the macroscopic and microscopic quantification together, under specific challenge conditions performed in this study, the sol-gel treated conditions were associated with reduced recovery of fluorescent Glo Germ material downstream of the test media. Since this study quantified material deposited on a downstream collector rather than measuring airborne particle concentrations upstream and downstream, these observations are appropriately interpreted as differences in relative fluorescent depositions, rather than standardized filtration efficiency measurements.

Estimated Glo Germ Challenge Magnitude

A separate spray deposition measurement was used to estimate the magnitude of fluorescent material generated by the Glo Germ spray. Within the concentrated deposition region produced by a 1-second spray, the microscopic analysis yielded approximately 1,768 fluorescent particles per 2 by 2 cm region. When scaled to the concentrated area of 25 by 25 cm, there was an estimate of about 276,250 fluorescent particles per 1-second spray. Assuming a constant spray output for the duration of the spray, this leads to approximately 1.38 x 106 particles per 5-second challenges used in painter's and N95 masks and 2.76 x 106 deposits for the 10-second challenges used in MERV 8 experiments. The area scaled for the total approximation was an estimate based on fluorescent deposition recovered on paper, not a direct measurement of total airborne particles emitted. These experiments provide an approximate quantification of the magnitude and consistency of the fluorescent challenge delivered during the filtration experiments.

Table 3. *Challenge magnitude with Glo Germ*

Challenge Condition	**Spray Duration (seconds)**	**Estimated fluorescent particles**
Calibration	1 second	~276,520

Challenge Condition	Spray Duration (seconds)	Estimated fluorescent particles
Painter's mask/N95	5 seconds	~1,381,250
MERV 8	10 seconds	~2,762,500

Discussion

The principal finding of this study was the consistent reduction in downstream deposition that can be tracked with fluorescence for filtration media that were treated with SCHN 135 when compared to their corresponding untreated trials. This pattern was observed across all three material categories that were tested: 1-inch MERV 8 HVAC filters, painter masks, and N95 respirators, and was evident with both UV-visible quantification and microscopic estimation. The similarity in results across three different filtration substrates and two independent measurement scales suggests that SCHN 135 treatment of these materials was capable of altering the transport and retention of the fluorescent challenge applied under the experimental conditions tested.

The magnitude of the observed reduction differed among filtration materials. The MERV 8 filters produced the largest decrease when treated with the sol-gel coating with an 89.6% microscopic decrease, whereas the painter's mask and N95 respirator trials showed a smaller but still consistent reduction in their downstream deposition. The painter's mask showed a significant decrease with an 81.5% microscopic decrease, as expected; however, the N95 masks did not exhibit a similar magnitude of decrease with 56.8% of microscopic particulates. While the hydrophobic treatment was capable of preventing more than 50% of microscopic particles from penetrating, the relative decrease was much smaller compared to painter's masks. There was still a downward trend compared to painter masks, indicating that SCHN 135 is effective in preventing passage, but the framework of the N95 masks is much stronger in capturing particulates without treatment compared to painter masks. However, the hydrophobic coating is capable of enhancing the strong

framework and preventing more particles from penetrating the mask. These differences are likely influenced by the inherent structure and filtration characteristics of the materials. Fibrous filters remove particles through several mechanisms, including inertial impaction, diffusion, interception, electrostatic interactions, and factors like fiber geometry, particle size, packing density, and airflow conditions can also affect filtration [16,17]. Surface treatment with SCHN 135 introduces an additional physicochemical modification to this existing filtration mechanism and may affect different materials to different extents.

Relationship to Previous Work

The observed reduction in downstream deposition is consistent with the broader principle that modification of the surface properties of the fiber structure of a filter can change the interactions between particles and filtration media. Previous work on SCHN 135 and related hydrophobic nanocoatings has demonstrated that sol-gel-derived surface coatings can modify textile and filtration surfaces while preserving the underlying structure [19]. Earlier work from Wang et al. using CaptureCoating reported reduced downstream recovery of the SARS-CoV-2 virus after the hydrophobic treatment of HVAC filtration media [28]. Related work from the Curran Nanophysics Research Group demonstrated the ability of SCHN sol-gel to reduce the water transport through porous materials, further supporting the potential for this material to be used in applications involving liquid particle transport [35]. These studies provide conceptual precedent for examining surface chemistry as an additional factor in the retention of particles.

Because CaptureCoating and SCHN 135 are distinct formulations, the earlier results cannot be interpreted as direct evidence of SCHN 135 performance. However, the previous findings provide useful conceptual precedent for the present study as these studies examined the effect of hydrophobic modification of the surface of substrates and transport of particles through it. The current work extends that broader research question by evaluating SCHN 135 independently and

by using a fluorescent nonbiological tracer that permits the visualization of deposition across HVAC filters and masks.

Limitations

This study was aimed to determine the effectiveness of SCHN 135 in preventing the passage of aerosol particulates, and potentially respiratory viruses as well. However, a respiratory virus was not utilized in experiments due to not having the appropriate resources to measure virus particulates.

While the SCHN 135 coating was capable of blocking the penetration of the aerosol particles in the study, it is uncertain whether respiratory viruses would demonstrate similar results. Having access to an RT-qPCR machine and other materials would allow for future trials to directly measure the coating's effectiveness on a respiratory virus.

In order to determine the efficiency of SCHN 135 coatings, filters and masks were sprayed and left to dry for 24 hours. However, after conducting a water test to examine hydrophobicity, certain areas either were not hydrophobic enough or had an insufficient coating, so a second coating was applied. To avoid this, a brief soaking in SCHN 135 may have allowed even coverage and ensured a proper coating was applied without interfering with the inner fibers of the filter. For future experimental trials, conducting soaking rather than spray applications may prove to yield more consistent coverage and allow for more consistent hydrophobicity across the filters and masks.

When conducting trials with the SCHN 135 coatings, it was noted that the nanomaterial was over five years old, which may have led to chemical degradation within the coating. Although the coating still proved to be effective in preventing passage of aerosol particles, there is potential that the coatings' full potential was not showcased throughout the experiments conducted. Therefore, it is possible that more particulates were capable of penetrating the hydrophobic surface

than anticipated. Future trials should be run with a newer solution to prevent potential chemical degradation.

Implications and Future Work

The consistent reduction in downstream deposition across all treated filtration materials supports further testing of SCHN 135 under more standardized conditions. Future experiments should use identical base materials, controlled coating application, measured airflow and pressure drop, repeated trials, and standardized image analysis. These improvements would allow particle penetration and filtration performance to be quantified more accurately and would also determine whether SCHN 135 changes airflow resistance. Additional measurements, such as contact angle and surface analysis, could be used to confirm the hydrophobicity and uniformity of the coating across the filter.

Most importantly, the experiment should be repeated using an appropriately controlled respiratory virus or virus-containing aerosol under suitable laboratory conditions and evaluated using RT-qPCR. This would allow the physical reduction in fluorescent tracer penetration observed in the present study to be tested for biological relevance and determine whether SCHN 135 can also reduce downstream transport of virus-containing respiratory particles.

Conclusion

This study demonstrates the effectiveness of SCHN 135 in capturing particulates on its surface and preventing passage for both filters and masks. Both UV-visible and microscopic imaging showed lower Glo Germ deposition downstream of every SCHN 135-treated condition when compared to its untreated trial. For the MERV 8 HVAC filter, treatment produced relative decreases of 98.2% in UV-visible deposition and 89.6% in microscopic deposition compared with the untreated filter.

Across the two mask materials, relative decreases ranged from 71.6% to 87.1% by UV-

visible measurements and from 56.8% to 81.5% by microscopic measurements. This aligns with the chemistry of the nanocoating in repelling polar liquids rather than absorbing them.

The results from this study conclude that SCHN 135 is capable of preventing water-based aerosol particles from penetrating treated materials. The importance of these findings lies in the relationship between respiratory viruses and water-based particle control. Since the majority of respiratory viruses travel via airborne water-based particles, this study demonstrates that reducing the amount of downstream deposition can act as a strategy for combatting any airborne water-based particles. However, since the present study did not evaluate the transport of an authentic biological virus, there is no direct effect by SCHN 135. Instead, these results establish a physical representation for investigating whether treated SCHN 135 filters and masks can influence the transport of respiratory viruses. This coating offers a cost-friendly, non-toxic, and viable option to protect households, buildings, and individuals from any liquid airborne particulates in the air. By reducing the penetration of aerosolized particles through masks and filters, nanomaterial-enhanced filtration may provide an additional layer of protection against cross-contamination and the airborne transmission of respiratory pathogens.

Acknowledgements

The authors gratefully acknowledge the members of the Curran Nanophysics Research Group (CNRG) for their assistance and support throughout this project. The authors also extend their sincere appreciation to Chris Taylor and Dr. Seamus Curran for their guidance, expertise, and continued support throughout this study.

References

[1] Leung, N. H. L. (**2021**). Transmissibility and transmission of respiratory viruses. *Nature Reviews Microbiology*, *19*(8), 528–545. https://doi.org/10.1038/s41579-021-00535-6

[2] Wang, C. C., et al. (**2021**). Airborne transmission of respiratory viruses. *Science*, *373*(6558), Article eabd9149. https://doi.org/10.1126/science.abd9149

[3] Morawska, L., Buonanno, G., Mikszewski, A., & Stabile, L. (**2022**). The physics of respiratory particle generation, fate in the air, and inhalation. *Nature Reviews Physics*, *4*(11), 723–734. https://doi.org/10.1038/s42254-022-00506-7

[4] Lindsley, W. G., et al. (**2010**). Measurements of airborne influenza virus in aerosol particles from human coughs. *PLoS ONE*, *5*(11), Article e15100. https://doi.org/10.1371/journal.pone.0015100

[5] Lindsley, W. G., et al. (**2015**). Viable influenza A virus in airborne particles from human coughs. *Journal of Occupational and Environmental Hygiene*, *12*(2), 107–113. https://doi.org/10.1080/15459624.2014.973113

[6] Thornton, G. M., et al. (**2023**). The impact of heating, ventilation, and air conditioning design features on the transmission of viruses, including the 2019 novel coronavirus: A systematic review of filtration. *PLOS Global Public Health*, *3*(9), Article e0002389. https://doi.org/10.1371/journal.pgph.0002389

[7] Patra, S. S., Nath, J., Panda, S., Das, T., & Ramasamy, B. (**2022**). Evaluating the filtration efficiency of commercial facemasks' materials against respiratory aerosol droplets. *Journal of the Air & Waste Management Association*, *72*(1), 3–9. https://doi.org/10.1080/10962247.2021.1948459

[8] Hlavinka, B., Robles Perez, A., Taylor, C., Wang, A., Nwaege, P., Maharjan, S., Russell, K., Scott, B., Gates, J., Curran, S. (**2026**). Environmental Virucidal Nanomaterials: An Overview of Efficacy and Mechanisms of Action. *Philosophy and Reason, 1(1), 88–108. https://doi.org/10.67644/pandr.v1i1.1872*

[9] Sublett, J. L., Seltzer, J., Burkhead, R., Williams, P. B., Wedner, H. J., & Phipatanakul, W. (**2010**). Air filters and air cleaners: Rostrum by the American Academy of Allergy, Asthma & Immunology Indoor Allergen Committee. *Journal of Allergy and Clinical Immunology*, *125*(1), 32–38. https://doi.org/10.1016/j.jaci.2009.08.036

[10] Corbin, J. C., et al. (**2021**). Systematic experimental comparison of particle filtration efficiency test methods for commercial respirators and face masks. *Scientific Reports*, *11*(1), Article 21979. https://doi.org/10.1038/s41598-021-01265-8

[11] Curran, S., Liao, S., Maharjan, S., Wang, A., Blau, W., Oremland, R., Metcalf, M., Taylor, C., Khan, M., Taylor, A., Du, M., Akande, F., Scott, B., & Russell, K. (**2026**). Future of Nanocomposites. *Philosophy and Reason*, *1*(1), 221–243. https://doi.org/10.67644/pandr.v1i1.1891

[12] Tsuda, A., Henry, F. S., & Butler, J. P. (**2013**). Particle transport and deposition: Basic

physics of particle kinetics. *Comprehensive Physiology*, *3*(4), 1437–1471. https://doi.org/10.1002/cphy.c100085

[13] Editorial Team for the Special Issue on Oosawa's Lectures. (**2023**). Chapter 8: Brownian motion. *Biophysics and Physicobiology*, *18*, S066–S075. https://doi.org/10.2142/biophysico.bppb-v18.s010

[14] Zhang, X., Yu, H., & Liu, J. (**2021**). Theoretical model of single fiber efficiency and the effect of microstructure on fibrous filtration performance: A review. *Industrial & Engineering Chemistry Research*, *60*(1), 3–36. https://doi.org/10.1021/acs.iecr.0c04400

[15] Yeh, H.-C., & Liu, B. Y. H. (**1974**). Aerosol filtration by fibrous filters—I. Theoretical. *Journal of Aerosol Science*, *5*(2), 191–204. https://doi.org/10.1016/0021-8502(74)90049-4

[16] Xu, Z. (**2013**). Filtration mechanism of fine particle. In *Fundamentals of air cleaning technology and its application in cleanrooms* (pp. 133–183). https://doi.org/10.1007/978-3-642-39374-7_3

[17] Rachmawati, I. Y., Hada, K., Shirzadi, M., Fukasawa, T., Fukui, K., & Ishigami, T. (**2024**). Investigation on the collection mechanism of van der Waals force in air filtration by numerical simulation and empirical model development. *Industrial & Engineering Chemistry Research*, *63*(23), 10410–10426. https://doi.org/10.1021/acs.iecr.4c00550

[18] Lee, K. W., & Liu, B. Y. H. (**1980**). On the minimum efficiency and the most penetrating particle size for fibrous filters. *Journal of the Air Pollution Control Association*, *30*(4), 377–381. https://doi.org/10.1080/00022470.1980.10464592

[19] Salinas, N., Chung, A., Falahat, R., Curran, M., Bell, J., Huynh, L., Paydar, A., Maharjan, S., Mellon, E., Russell, K., & Curran, S. (**2026**). Self-Cleaning Hydrophobic Nanocoatings on Textiles- Evaluating SCHN 135 and CaptureCoating. *Philosophy and Reason*, *2*(1), 100–123. https://doi.org/10.67644/pandr.v2i1.1847

[20] Curran, S., Mellon, E., Ali, R., Maharjan, S., Gates, J., Taylor, C., Scott, B., & Russell, K. (**2026**). Solving Structural Degradation and Reducing Financial Risk in Masonry via Nano-Silane Based Polymer Nanocoating's. *Philosophy and Reason*, *2*(1), 9–41. https://doi.org/10.67644/pandr.v2i1.1843

[21] Hasimbegovic, H., Chaudhry, I., Holeman, L., & Curran, S. (**2026**). Hydrophobic Effect of Self-Cleaning Hydrophobic Nanocoating on Wooden Materials. *Philosophy and Reason*, *2*(1), 124–150. https://doi.org/10.67644/pandr.v2i1.1848

[22] Hench, L. L., & West, J. K. (**1990**). The sol-gel process. *Chemical Reviews*, *90*(1), 33–72. https://doi.org/10.1021/cr00099a003

[23] Akande, F., Rojas, P., Salinas, N., Taylor, C., Bao, J., Qin, C., & Curran, S. (**2026**). Inhibition of Sulfate-reducing Bacteria Presence in Masonry via High-Performance Sol-Gel Coatings. *Philosophy and Reason*, *2*(1), 74–99. https://doi.org/10.67644/pandr.v2i1.1869

[24] World Health Organization. (n.d.). *The true death toll of COVID-19: Estimating global excess*

mortality. Retrieved August 27, 2026, from https://www.who.int/data/stories/the-true-death-toll-of-covid-19-estimating-global-excess-mortality

[25] Liveris, A., et al. (**2022**). When New York City was the COVID-19 pandemic epicenter: The impact on trauma care. *Journal of Trauma and Acute Care Surgery*, *93*(2), 247–255. https://doi.org/10.1097/TA.0000000000003460

[26] Kariya, T. (**2020**). Rapid spread of COVID-19 in New York and the response of the community. *Global Health & Medicine*, *2*(2), 123–126. https://doi.org/10.35772/ghm.2020.01032

[27] Mellon, E., Russell, K., Scott, B., Wang, A., Maharjan, S., Gates, J., & Curran, S. (**2026**). The Philosophy of Thought and Scientific Logic Tackling Covid 19. *Philosophy and Reason*, *1*(1), 15–29. https://doi.org/10.67644/pandr.v1i1.1856

[28] Wang, A. J., Maharjan, S., Russell, K., Scott, R., Mellon, E., & Curran, S. A. (**2021**, January). *Preventing indoor transmission of airborne SARS-CoV-2 via HVAC systems: A virus-capturing hydrophobic nanocoating for air-filtration media* [Internal technical report]. CNTG, Advanced Manufacturing Institute, University of Houston and Curran Biotech.

[29] Johnson, D. L., & Lynch, R. A. (**2008**). An efficient analytical method for particle counting in evaluating airborne infectious isolation containment using fluorescent microspheres. *Journal of Occupational and Environmental Hygiene*, *5*(4), 271–277. https://doi.org/10.1080/15459620801935056

[30] Patel, S. H., Yim, W., Garg, A. K., Shah, S. H., Jokerst, J. V., & Chao, D. L. (**2020**). Assessing the physiological relevance of cough simulators for respiratory droplet dispersion. *Journal of Clinical Medicine*, *9*(9), Article 3002. https://doi.org/10.3390/jcm9093002

[31] Shah, S. H., Garg, A. K., Patel, S., Yim, W., Jokerst, J. V., & Chao, D. L. (**2021**). Assessment of respiratory droplet transmission during the ophthalmic slit-lamp exam: A particle tracking analysis. *American Journal of Ophthalmology*, *222*, 76–81. https://doi.org/10.1016/j.ajo.2020.08.046

[32] Glo Germ Company. (n.d.). *Glo Germ MIST Kit Basic (Model KTMST)*. Retrieved August 27, 2026, from https://www.glogerm.com/mm5/merchant.mvc?Screen=PROD&Product_Code=KTMST

[33] AC Infinity Inc. (n.d.). *CLOUDLINE T10, quiet inline fan 10" with temperature, humidity, VPD controller*. Retrieved August 27, 2026, from https://acinfinity.com/cloudline-t10-quiet-inline-fan-10-with-temperature-humidity-vpd-controller/

[34] Rossner, M., & Yamada, K. M. (**2004**). What's in a picture? The temptation of image manipulation. *Journal of Cell Biology*, *166*(1), 11–15. https://doi.org/10.1083/jcb.200406019

[35] Kabani, S., Khan, M., Akande, F., Russell, K., Taylor, C., Gates, J., & Curran, S. (**2026**). Sol-Gel Coatings Masonry Sealer for PFAS-Replacement Coatings that Reduces Sorptivity, Acid-Induced Degradation, and Internal Steel Corrosion in Masonry Materials. *Philosophy*

and Reason, *2*(1), 42–73. https://doi.org/10.67644/pandr.v2i1.1844